STATISTICAL CHARACTERISTICS FOR THE BACKGROUND NOISE IN DISTRIBUTED ACOUSTIC SENSING: ANALYSIS AND APPLICATION TO SUPPRESSION

T. ZHONG[1,2], Y. CHEN[2] , X.T. DONG[3], Y. LI[4*] and N. WU[4]

[1] *Key Laboratory of Modern Power System Simulation and Control and Renewable Energy Technology, Jilin 132012, P.R. China. 519647817@qq.com*
[2] *Northeast Electric Power University, Department of Communication Engineering, Jilin 132012, P.R. China. 2451184169 @qq.com*
[3] *Jilin University, College of Instrumentation and Electrical Engineering, Changchun 130026, P.R. China. 18186829038@163.com;*
[4] *Jilin University, Department of Information Engineering, Changchun 130026, P.R. China. liyue@jlu.edu.cn*

(Received February 13, 2021; revised version accepted December 6, 2021)

ABSTRACT

Zhong, T., Chen, Y., Dong, X.T., Li, Y. and Wu, N., 2022. Statistical characteristics for the background noise in distributed acoustic sensing: analysis and application to suppression. *Journal of Seismic Exploration*, 31: 131-151.

Distributed acoustic sensing (DAS) is a novel technology that utilizes a fiber-optic cable instead of geophones, which has attracted increasing attention in seismic data acquisition. However, owing to the existence of background noise, the current quality of the DAS records requires improvement. In this study, the stationarity and spectral characteristics for DAS background noise are investigated. Additionally, the dataset used for the analysis is collected while satisfying the practical requirements of the exploration industry. The results demonstrate that the DAS background noise is a broadband interference with local stationarity. On this basis, an adaptive time-frequency peak filtering (TFPF) algorithm is proposed to attenuate the background noise. Unlike traditional TFPF algorithms, this improved method adaptively chooses appropriate filtering parameters instead of using a fixed parameter set to the whole seismic record to achieve better attenuation performance. Specifically, the signal and noise segments can be recognized by taking advantage of the differences in stationarity. Consequently, we can adaptively select different filtering parameters for signal and noise segments to get better performance in noise attenuation and signal restoration. Synthetic and field data experimental results indicate that the proposed adaptive TFPF algorithm can suppress the DAS background noise and accurately recover the reflection events, especially under low signal-to-noise ratio conditions.

KEY WORDS: distributed acoustic sensing, background noise attenuation, time-frequency peak filtering, seismic data processing.

0963-0561/22/$5.00

NOMENCLATURE

Acronyms

DAS	Distributed Acoustic Sensing
EMD	Empirical Mode Decomposition
FCL	Fractal Conservation Law Method
IF	Instantaneous Frequency
IMFs	Intrinsic Mode Functions
MT	Multitaper
PWVD	Pseudo Wigner–Ville Distribution
PSD	Power Spectral Density
RMSE	Root Mean Squared Error
SNR	Signal-to-noise Ratio (dB)
TFPF	Time-Frequency Peak Filtering
WL	Window Length

INTRODUCTION

Distributed acoustic sensing (Mateeva et al., 2014; Parker et al., 2014; Spikes et al., 2019) is a novel acquisition technology that utilizes the optical scattering response of a laser pulse to record the strain changes caused by seismic waves (Hartog, 2018). Comparing to conventional point-receiver recording systems, DAS can simultaneously sense the entire length of the utilized optical fiber cable. It may have many applications from a data acquisition perspective (Binder et al., 2020; Rodrigue et al., 2020), especially in the oil and gas industry (Daley et al., 2016; Gotz et al., 2018). In addition, it is shown that the DAS array has a spatial resolution at meter scale and continuous temporal samplings (Verdon et al., 2020; Bellefleur et al., 2020). Hence, DAS is increasingly recognized as a viable alternative to geophone arrays owing to its advantages in deployment and spatial coverage (Poletto et al., 2016; Harris et al., 2017; Karrenbach et al., 2019). However, the background noise in DAS records usually contains many incoherent interferences, such as the broadband noise caused by the optical scattering process (Gang et al., 2018; Bellefleur et al., 2020), which results in a relatively low SNR for the DAS records, even lower than those obtained with geophones in some conditions (Correa et al., 2017). Additionally, some of these incoherent interferences are not issues in conventional seismic records, such as time-variant optical noise and fading noise. Specifically, all these types of incoherent interferences, brought by optical transmission process and recording instruments, have different representation fashions and statistical properties with conventional seismic random noise. It means that the attenuation methods applied in conventional seismic data processing may degenerate when dealing with complex DAS records. To improve the quality of the DAS data, efficient background-noise attenuation approaches have attracted increasing attention in geophysics.

It is known that the denoising procedure is important for obtaining higher accuracy seismic data. In DAS data processing, the background noise is assumed to be zero-mean and broadband in nature (Riedel et al., 2018), and then a series of processing algorithms have been applied. The currently used denoising algorithms, such as weighted-mean stack (Gang et al., 2018; Kobayashi et al., 2020), linear filtering techniques (Soto et al., 2016), and 2D rectangular band-pass filters (Matins et al., 2019), are relatively oversimplified. However, the performance of these methods may degenerate when dealing with complicated DAS records. Moreover, owing to the lack of accurate understanding of the noise properties, the application of modern noise reduction methods is unfeasible. Thus, an important step for resolving the problem is to further investigate the properties of the DAS background noise for selecting or designing efficient noise reduction methodologies.

Here, the statistical characteristics of the DAS background noise are analyzed, including stationarity, PSD, and an adaptive denoising algorithm is proposed by utilizing its corresponding features. Herein, stationarity refers to the wide-sense stationary, which only requires the first and second order of statistical moments to be time-invariant (Chatfield, 2003). Moreover, the PSD represents the amount of energy described by a time series when transformed into a spectral function (Zhong et al., 2015). In addition, the statistical properties of the DAS background noise have not been scientifically studied yet, and thus far, the corresponding published evidence is rare. However, we could obtain necessary references from similar research in the field of conventional seismic data processing. The inherent assumption is that the recorded noise should have similar properties due to the affinity of the acquisition environmental characteristics. Recently, some research has indicated that the background noise, acquired by conventional geophones, forms a non-stationary and non-Gaussian stochastic process, whereas its main energy concentrates in the low-frequency bands (Zhong et al., 2015; Li et al., 2017; Zhong et al., 2019). Based on these findings, some denoising algorithms have been presented and successfully applied in seismic data processing (Jiang et al. 2014; Zhang et al., 2015; Dong et al., 2018). However, the aforementioned findings cannot directly represent DAS noise characteristics because of the broad frequency band of DAS noise compared to conventional seismic data. Thus, we need to intensively analyze the actual properties of the DAS background noise by combining the existing results obtained from conventional seismic data. To the best of our knowledge, this work is one of the first attempts to investigate this problem.

In this study, the stationarity for DAS noise is investigated by applying a testing method based on time-frequency analysis (Souza et al., 2013), and the PSD is analyzed based on the MT spectral estimation algorithm (Thomson, 1982; Bayram and Baraniuk, 2000). The corresponding methods have already been successfully used in signal processing (Ardekani et al., 2013) and seismic data analysis (Zhong et al., 2015). Moreover, the used dataset was collected under the actual course of seismic exploration. We also propose an adaptive denoising algorithm based on TFPF (Boashash and Mesbah, 2004; Wu et al., 2011), which is an efficient noise reduction

method in conventional seismic data processing. In addition, a series of experiments were conducted to verify the effectiveness of the proposed method. We provide detailed descriptions of the dataset and analysis principles in the following section.

METHOD AND THEORY

In this section, we provide a detailed description of the basic principles of the stationarity testing method and conventional TFPF algorithm used in this study.

Frameworks of the stationarity testing method

It is established that the characteristics of a non-stationary series evolve in time, such as time-variable energy distributions or vibratory fashions. Thus, the stationarity can be evaluated by verifying the existence of a significant trend component in the time–frequency domain. The procedures of the stationarity testing method can be concluded as follows:

1. Obtain the energy distributions of the test series

The energy distribution can be denoted as the time marginal, defined by the following equation:

$$F(t) = \sum_{m=1}^{M} S_K(t, f_m) \quad , \tag{1}$$

where $S_k(t,f_m)$ is the time-frequency distributions for the analysed series $x(t)$, which is obtained by multitaper spectrogram method:

$$S_K(t, f) = \frac{1}{K} \sum_{k=0}^{K-1} \left| \int x(l) h_k(l - t) e^{-2\pi i f l} dl \right|^2 \quad , \tag{2}$$

where the symbol $h_k(t)$ represents the k-th Hermite function, whose length is T_h.

2. Extracting the trend components of the energy distributions.

On this basis, EMD is applied to divide the $F(t)$ into IMFs $M_i(t)$ and a residual. The trend $c(t)$ can be represented by combining the IMFs and the residual $\rho_I(t)$, which is shown as follows:

$$c(t) = \sum_{i=i^*}^{I} M_i(t) + \rho_I(t) \quad .$$

3. Here, the optimum index i^* can be determined by the energy-ratio method (Moghtaderi et al., 2013). Measure the stationarity of the test series.

The test statistic Φ, which is used to represent the stationarity, can be obtained by the ratio of the following variance:

$$\Phi = \frac{Var(F(t))}{Var(F(t)-c(t))} = \frac{\sum_{t=1}^{n}\left[\sum_{i=i^*}^{I} M_i(t) + \rho_I(t) - \mu_F\right]^2}{\sum_{t=1}^{n}\left\{\left[\sum_{i=i^*}^{I} M_i(t) + \rho_I(t) - \mu_F\right] - \left[\sum_{i=i^*}^{I} M_i(t) + \rho_I(t) - \mu_F\right]\right\}^2} \quad . \quad (4)$$

It is established that if there is no evident trend component, Φ should be close to 1 (Flandrin et al., 2004). Thus, in this study, we use 2 as the threshold for the stationarity testing algorithm.

Principles of the TFPF algorithm

It is always assumes that the reflection signal $x(t)$ is contaminated with additive noise $n(t)$ in seismic data processing. Moreover, it is found that the signal $x(t)$ can be represented as the summation of valid components $x_i(t)$ with overlapping frequency spectra. Thus, the observed noisy signal $s(t)$ can be denoted as follows:

$$s(t) = x(t) + n(t) = \sum_{i=1}^{p} x_i(t) + n(t) \quad (5)$$

The basic procedures for TFPF can be concluded as follows. First, the noisy signal is encoded to the IF of an analytic signal, and then the desired signal is recovered by IF estimations. In addition, the encoding procedure can be accomplished by employing the following equation:

$$Z_S(t) = e^{j2\pi\mu\int_0^t s(\lambda)d\lambda} \quad , \quad (6)$$

where $Z_S(t)$ is an analytical signal and μ is a scaling parameter. In this study, μ was set to 0.75. Moreover, the time–frequency distribution for the given analytical signal is calculated through the PWVD. The results can be denoted as follows:

$$PW_{Z_S}(t,f) = \int_{-\infty}^{\infty} h(\tau) Z_s(t+\frac{\tau}{2}) Z^*{}_s(t-\frac{\tau}{2}) e^{-j2\pi f\tau} d\tau \quad , \quad (7)$$

where $h(\tau)$ represents the window function. Based on this, by searching the peak value from the time–frequency plane, the filtered signal $\hat{x}(t)$ can be obtained as follows:

$$\hat{x}(t) = \frac{\arg\max_{f}[PW_{z_s}(t,f)]}{\mu} \quad . \tag{8}$$

Notably, the filtering performances for TFPF is related to the properties of the window function. The filtering result is sensitive to the WL of $h(\tau)$ and the dominant frequency of the analyzed signal. Evidently, a long WL generally indicates better noise reduction effects, but worse preservation in signal amplitudes. Fig. 1 shows the comparisons between the different filtering results. In the figure, a simulated signal (grey line) is contaminated by Gaussian noise with a SNR of 0 dB, whereas the filtering results with WL = 7 and WL = 21 are shown as the red line and black line, respectively. The figure indicates that the result obtained with WL = 21 can significantly reduce the noise with a significant loss in amplitude of the recovered signal, whereas the results for WL = 7 present the contrasting conclusions. Thus, we can conclude that the processing results for the TFPF algorithm might be balanced between noise reduction and signal preservation by amending the WL.

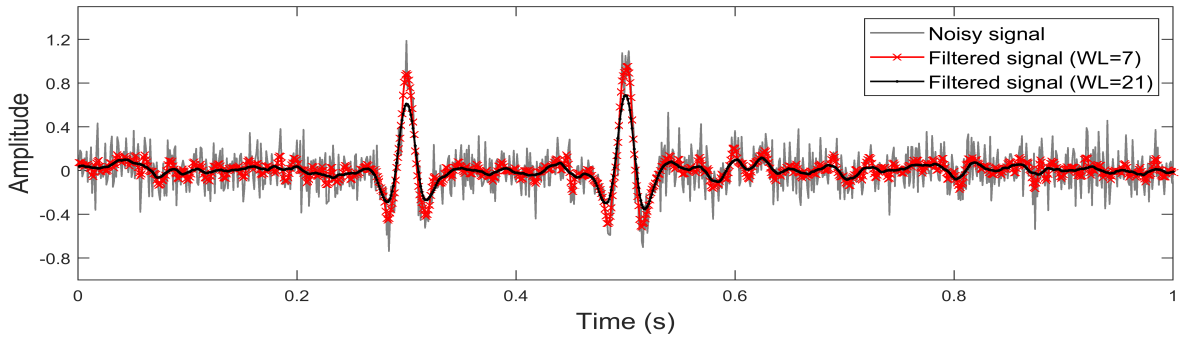

Fig. 1. The comparisons between filtering results with different parameters.

DAS NOISE CHARACTERISTICS ANALYSIS

In this section, we provide a brief description of the dataset, including detailed information for the acquisition conditions. On this basis, the stationarity and PSD properties of DAS noise are analyzed by applying the aforementioned stationarity testing algorithm and spectral estimation method. Additionally, we make a detailed comparison between the features of the signal and background noise, which would provide references for the designing of the noise reduction method in the following section.

Description of the dataset

Recently, DAS has been proven to be feasible for acquiring seismic data at high temporal and spatial resolutions. In general, DAS systems are

commonly based on the Rayleigh backscattering of laser pulses. During the recording procedure, the seismic wave may stretch or squeeze the optical fiber; then, the strain changes are recorded by the reflected photons. In this study, the field DAS acquisition was conducted under the operation of the exploration industry in September 2018. We collected the DAS records in an onshore well in Northeastern China by using wireline-conveyed fibers. The length of the optical fiber is 1100 m. Each record has 1000 channels, whereas the channel spacing is 1.02 m and the sampling frequency is 1000 Hz. In addition, the acquisition system continuously records for 15 s every minute, and consequently, 50000 trace records are obtained. Table 1 gives the detailed parameters for the acquisition system. Because the acquisitions are performed in remote areas, the artificial background noise is relatively insignificant. Consequently, the quality of the DAS records can be guaranteed. Fig. 2 displays a 12 s-long field DAS noise record, and it can be observed that no evident coherent noise is visible in the figure.

Table 1. Collection parameters for acquisition system.

Parameters	Specifications
Sampling frequency	1000Hz
Trace interval	1.02m
Trace numbers for acquisition system	1000
Acquisition strategy	Continuously collecting 15s for every minute
Total trace records	50000

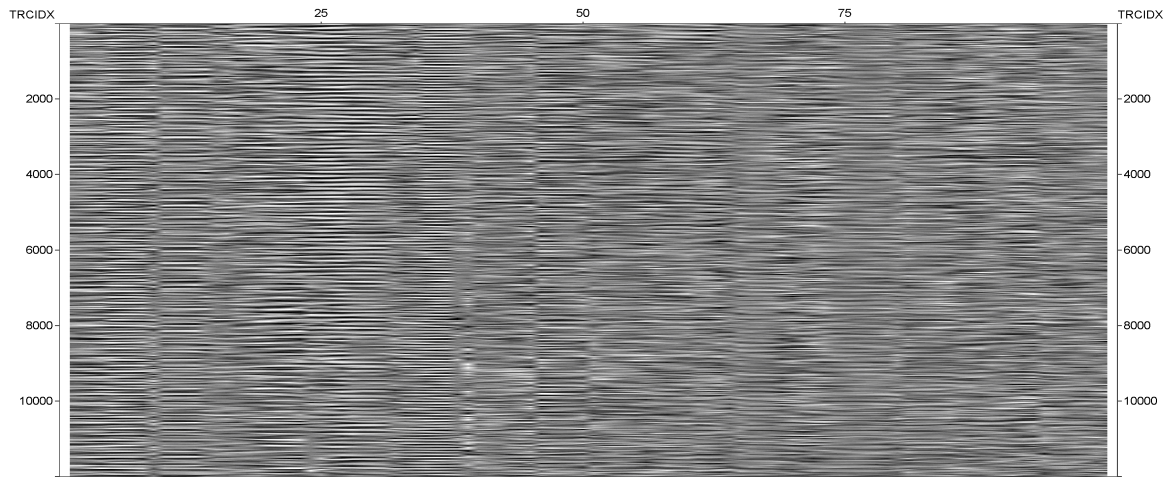

Fig. 2. The field DAS background noise data (12s-long and 100 trace).

Stationarity property analysis

In this study, the stationarity for DAS background noise is analyzed, and we also compare them with reflection signals. In geophysics, stationarity could reflect the stability of the acquiring environment. If the environment varies, it means that the noise properties might be modified and the stationarity may degrade. Thus, we can infer that the noise collected in a complicated environment may have strong non-stationarity. By applying the aforementioned testing method, typical background noise and field noise signal series are processed, and the stationarity analysis results are shown in Fig. 3. In Fig. 3(a), the waveform for a DAS noise series is provided, and we can observe that the noise series fluctuates in a nearly consistent fashion. By utilizing the testing statistic, the noise is classified as a stationary series. In contrast, the noise and signal series shown in Figs. 3(b) and 3(c) depict a time-variant fluctuation scope and severe changes in vibratory fashion, while conspicuous trend components are existed in PSD. Moreover, the stationarity statistics for them are 2.28 and 3.24, which are all greater than the threshold. Thus, the corresponding noise and signal series were tested to be non-stationary. By analyzing the dataset, numerous non-stationary noise series are obtained, indicating that the background noise is not strictly stationary. Furthermore, it is also intuitively observed that noisy signals have stronger non-stationary features.

On this basis, the stationarity of the dataset under different durations was investigated. This means that the stationarity evolution with time is studied, which can provide a specific reference for designing the denoising method. Herein, we mainly concentrate on the properties for short data, and the results for the background noise and noisy signals are shown in Fig. 4. Notably, the non-stationary proportions for the background noise under different durations are relatively low, with only 9.8% for a 0.5 s series. In contrast, the non-stationary proportions for the noisy signals are beyond 84%. All these results indicate that the noise data are superior to the noisy signals in terms of stationarity. In other words, we can deduce that the noise series could be considered as local-stationary, and short noise series always has better stationarity. On this basis, it is also reasonable to assume that the presence of the effective signals breaks the stationarity of the noise data. More importantly, the differences in stationarity could be utilized to recognize the reflection signals, which provide foundations for the adaptive filtering parameter strategy.

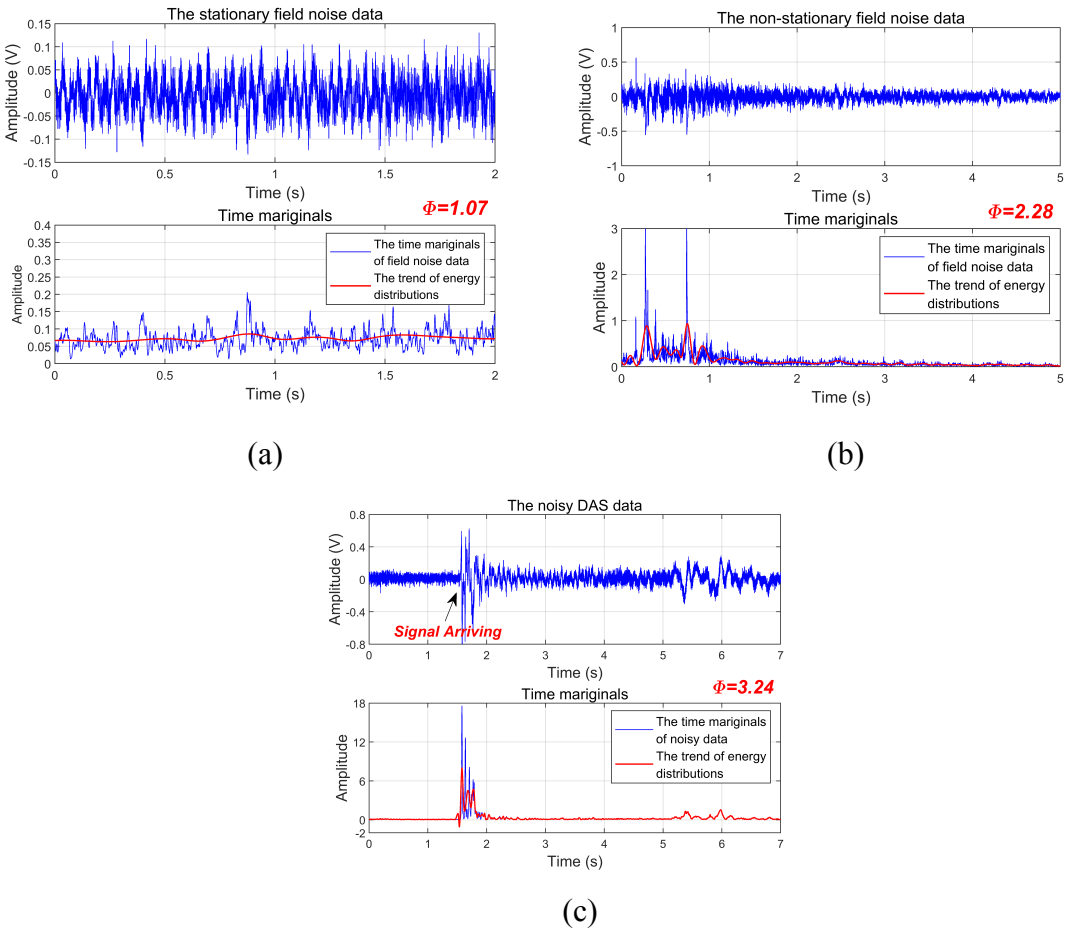

Fig. 3. The stationarity testing results for the analyzed data. (a) and (b) Noise series with different stationarity. (c) A field noisy signal which is classified as non-stationary series.

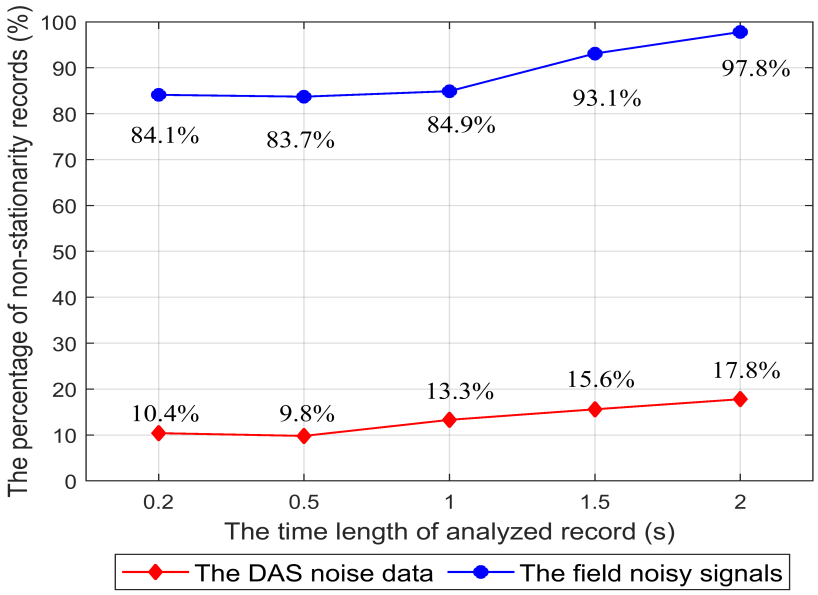

Fig. 4. The comparisons between the stationarity for noise and effective signal records in different time lengths (signal, line with blue spots; noise, line with red rhombus).

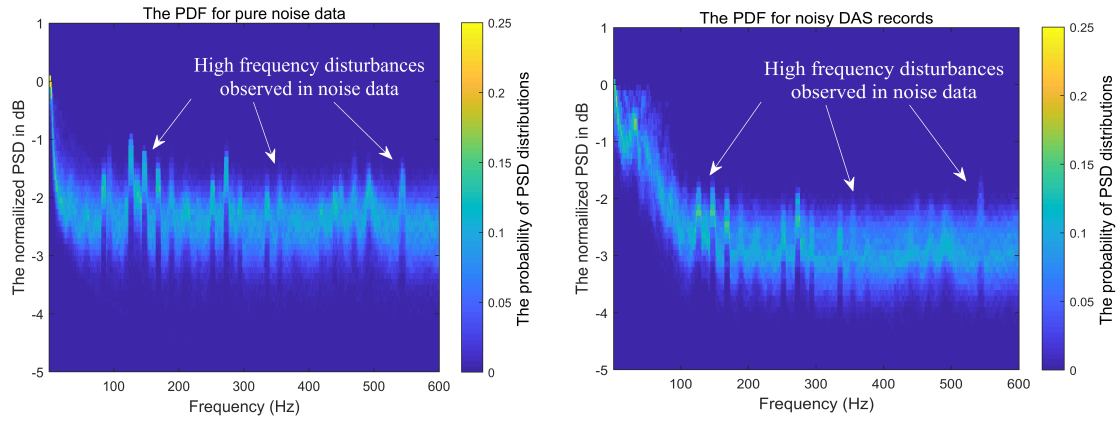

(a) (b)

Fig. 5. The spectral cumulative distribution for the noise data and noisy signal. (a) The results for the noise data. (b) The results for the field noisy record.

Spectral properties

Spectral properties were used to investigate the characteristics of the energy distributions in the frequency domain. Herein, we use the MT spectral estimation method to analyze the PSD, and the estimation results for a given series x(n) can be represented as follows (Thomson, 1982):

$$S_{x,m}(f) = \frac{1}{K_m}\sum_{k=1}^{K_m}\left|\sum_{n=0}^{N-1} d_k(n)x(n)e^{-2\pi fn}\right|^2 \quad , \tag{9}$$

where $d_k(n)$ represents the window function, which is selected from the discrete prolate spheroidal sequences, and K_m indicates the number of the analyzed window functions. Evidently, the MT method has advantages over traditional spectral estimation algorithms, such as the Welch algorithm, in spectral leakage, estimation variance, and frequency resolution. By applying the MT method, the normalized PSD is calculated, and the spectral cumulative distribution for the noise data and noisy signals are shown in Fig.5. Notably, DAS noise has a broader band with large amount of high-frequency disturbances than the noise acquired in traditional seismic arrays. Similarly, high-frequency components could still be observed in the PSD for noisy signals. In contrast, the main differences in the PSD results exist in the low-frequency bands where noisy signals have more components in the range of 0-70 Hz. Thus, we can deduce that the dominant frequency for the DAS signal should fall into the aforementioned scope. To verify the findings, a typical noisy signal, divided into a noise segment and two signal segments, is analyzed, and the results are shown in Fig. 6. It is observed that high-frequency harmonic components can also be found in the signal segments. Thus, we can determine that the DAS noise contains high-frequency disturbances, and the dominant frequency for the signal is relatively low. Based on these findings, it is suggested that low-frequency components should be preserved for recovering the reflection signals in the filtering procedure.

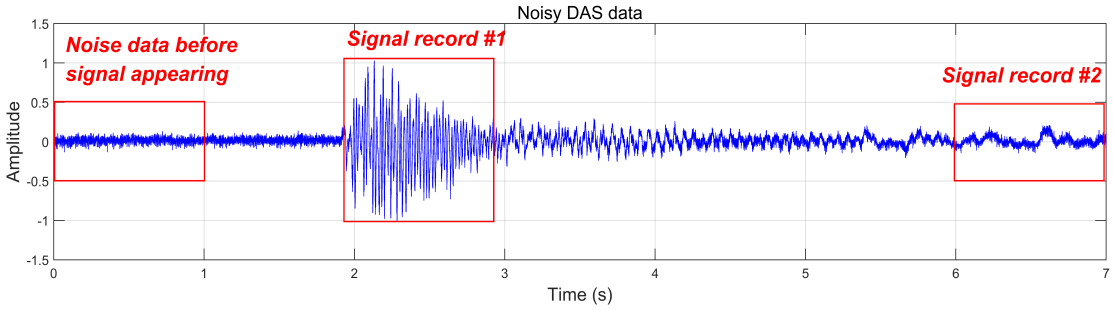

(a)

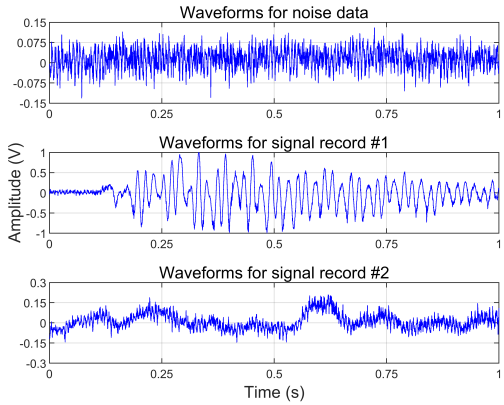

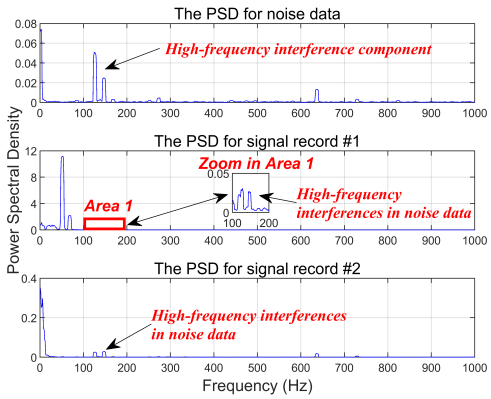

(b) (c)

Fig. 6. The comparisons between noise and effective signals. (a) The waveforms for a 7-second-long field DAS record. (b) The waveforms for noise data and signal segments. (c) The corresponding PSD for the aforementioned data.

ADAPTIVE TFPF METHOD AND PROCESSING RESULTS

In this section, we give the principle for the filtering algorithm and use a series of experiments to check the performance of the proposed method.

Principle for the denoising algorithm

As aforementioned, it is shown that the DAS background noise, which is a broadband disturbances with high-frequency components, has different properties in stationarity by comparing with efficient signals, and it can be used to design the denoising algorithm. Particularly, the signal segments should be detected by utilizing the differences in stationarity between noise and signal. On this basis, different filtering parameters are chosen for the analyzed DAS records to attenuate the noise purposefully. The denoising procedures for the adaptive TFPF method could be concluded as the flowchart shown in Fig. 7. To check the feasibility, a synthetic trace record contaminated with field background noise is processed, and the corresponding results are shown in Fig. 8.

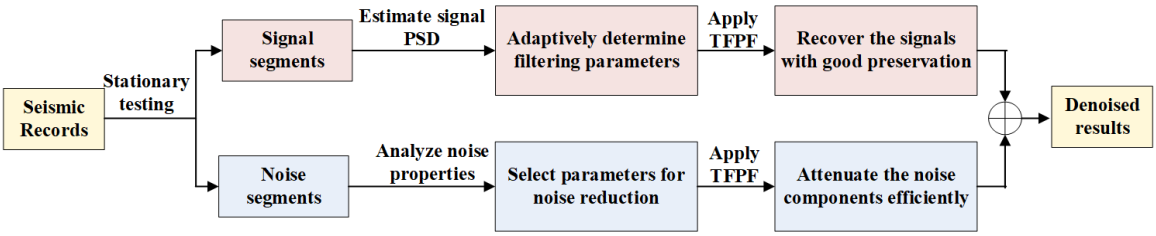

Fig. 7. Basic flow for the adaptive TFPF method proposed in this study.

The noisy record is divided into segments, whose length is set to 40 samples, and the stationarity for each segment is analyzed. Fig. 8(a) shows the waveforms, PSD, and stationarity testing results for a given noisy signal. It is shown that the background noise is represented as a high-frequency fluctuation, and the signal is severely influenced by the strong noise. By applying the testing method, the signal segments could be identified owing to their large testing statistics. As discussed in the Methods section, the performance for TFPF can be modified by controlling the window length to make a balance between noise reduction and signal restoration (Wu et al., 2011). As the signal segments have already been recognized, we can use different filtering parameters in different areas to attenuate the noise. Herein, we propose an adaptive WL selection strategy as shown in the following equation:

$$WL_{opt} = 0.125 f_s / f_d + \gamma \cdot \sigma_n / \xi_n \quad (10)$$

,,,

where f_d and f_s denote the dominate frequency of the analyzed signal and sampling frequency of the DAS record, respectively. Moreover, ξ_n and σ_n represent the mean and variance for the normalized data, while γ is a binarization function, whose value for the signal and noise segments is set to be 0 and 5. Thus, we can use short WL in signal segments to get better signal preservation, and apply long WL in noise segments to achieve thoroughly noise attenuation. For analyzing the efficiency of the proposed method, a synthetic record is processed, whereas the WL for signal and noise segments are 5 and 60, respectively. Additionally, we compare the processing results with the conventional TFPF algorithm. By observing the results shown in Fig. 8(b), adaptive TFPF has better performance than conventional TFPF (WL = 13) in terms of both noise reduction and signal preservation. Specifically, the corresponding results demonstrate that the proposed algorithm can suppress the noise by considering signal preservation is based on the fact that different filtering parameters are used in noise and signal segments. Therefore, we can determine that our proposed method can eliminate the background noise and restore the desired signals, even under strong noise conditions.

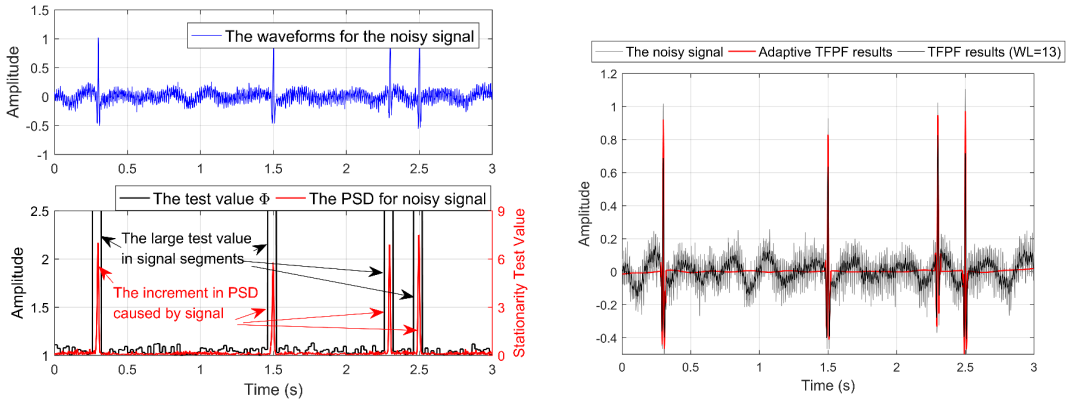

(a) (b)

Fig. 8. The signal recognition and denoising results of the proposed method. (a) The signal recognition result. (b) The comparison between noisy signal and its denoising result.

Synthetic DAS record processing results

Herein, we investigate the processing accuracy of the proposed method by comparing it with the common denoising algorithms used in seismic data processing. Specifically, the wavelet, FCL (Azerad et al., 2012; Meng et al., 2015), and conventional TFPF algorithm are used as the competing algorithms. Moreover, the synthetic DAS record, shown in Fig. 9(a), is used as the analyzed dataset. The first arrival and four reflection events have the same dominant frequency of 50 Hz and different apparent velocities of 1300 m/s and 1500 m/s, respectively. On this basis, field DAS background noise is added to the synthetic records and the reflection events are badly influenced by the severe background noise. By evaluating the stationarity, the reflection events are recognized well owing to their large stationarity statistics [shown in Fig. 9(b)], which provide a solid foundation for further denoising procedures.

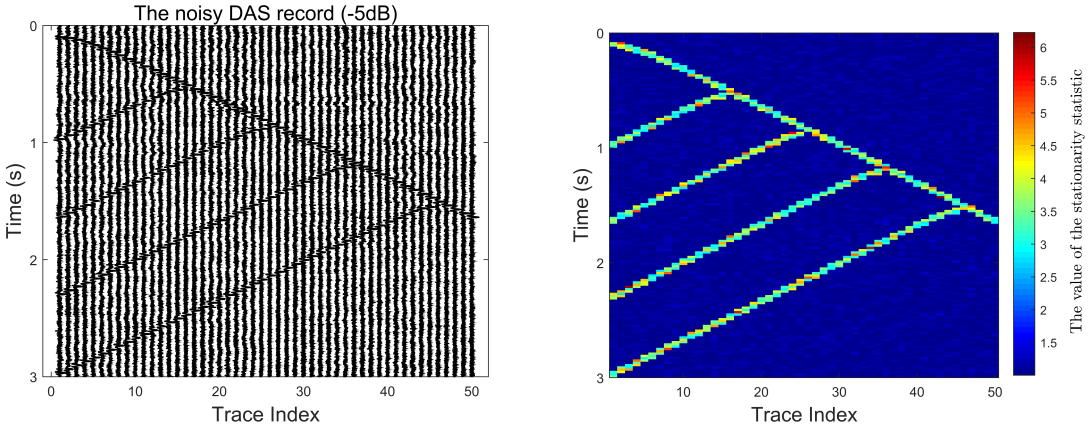

(a) (b)

Fig. 9. The signal recognition results by analysing stationarity. (a) The noisy DAS record. (b) The recognition result.

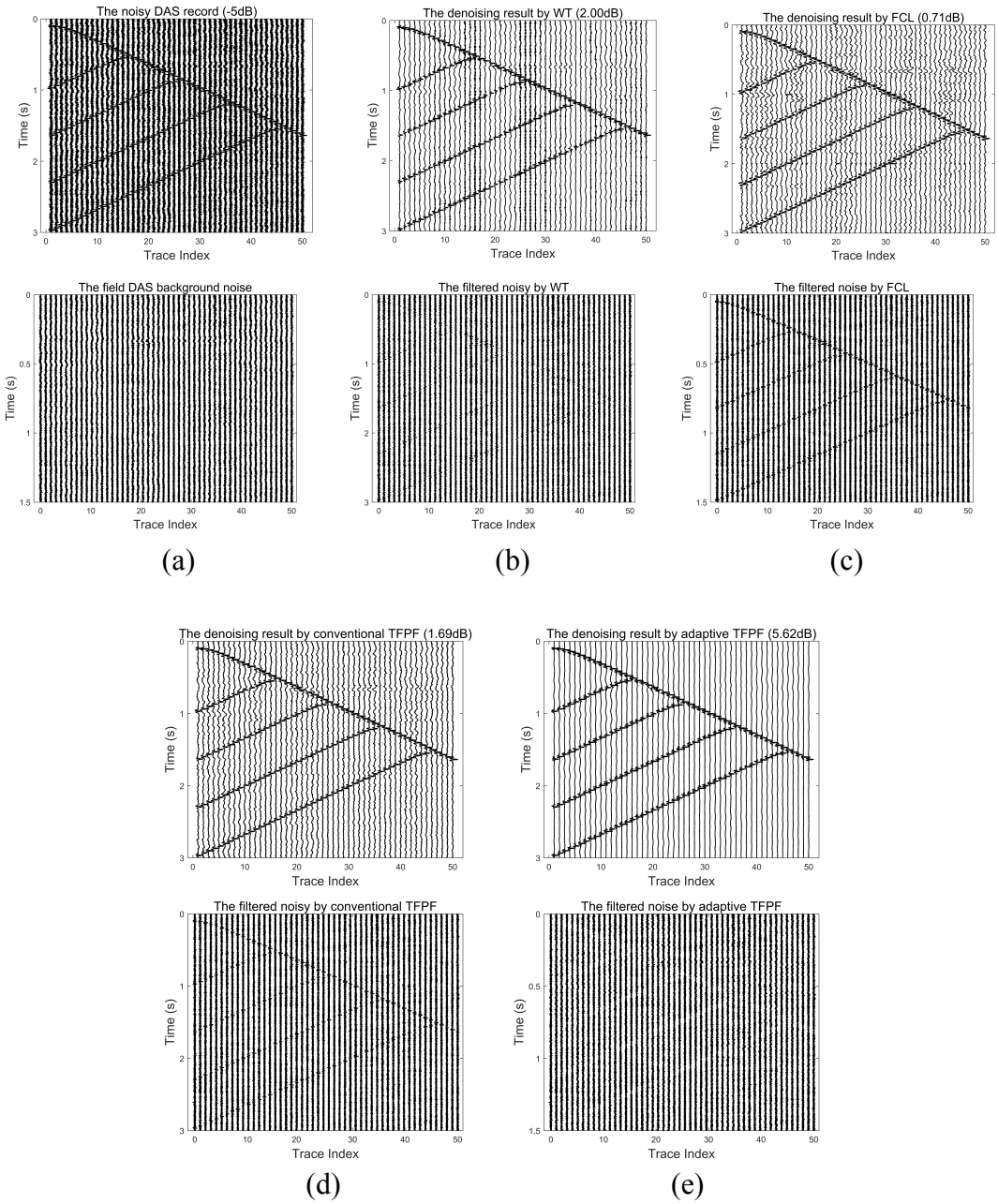

Fig. 10. Comparisons for denoising results and filtered noise. (a) Synthetic record (-5dB) and added noise acquired from field dataset. (b) Denoising results of WT (2.0dB). (c) Denoising results of FCL (0.71dB). (d) Denoising Results of TFPF (1.69dB) (e) Denoising results of adaptive TFPF (5.62dB).

For further analyzing, different noise attenuation algorithms are utilized to mitigate the strong background noise, and the corresponding denoising results are shown in Fig. 10. Herein, WT decomposition method with 5 layers of db5 base function is applied. Additionally, the filtering parameter for FCL is set to be [0.0145, 0.0201, 1.9], and the WL for the conventional TFPF is 11. In contrast, the proposed adaptive TFPF method applies WL = 5 for signal segments and WL = 40 for noise segments. The synthetic noisy DAS record (-5 dB) and the added field DAS background noise data are shown in Fig. 10(a). The results shown in Fig. 10(b) indicate that the WT

could attenuate the noise well; however, the continuity of the reflection events is destroyed in some areas. Similarly, although the FCL and conventional TFPF can suppress the noise better with an SNR of 0.71 and 1.69 dB, they have a large amount of residual signals remained in the filtered noise, as shown in Figs. 10(c) and 10(d). In contrast, the proposed adaptive TFPF can attenuate the noise appropriately, and no conspicuous signals remain in the filtered noise, as shown in Fig. 10(e). By observing the figures, we can infer that the adaptive TFPF suppresses the background noise more thoroughly and restores the effective signal more accurately. In addition, the quantitative comparisons in the improved SNR verify the efficiency of the proposed adaptive TFPF method, which has the largest SNR increment of over 10 dB.

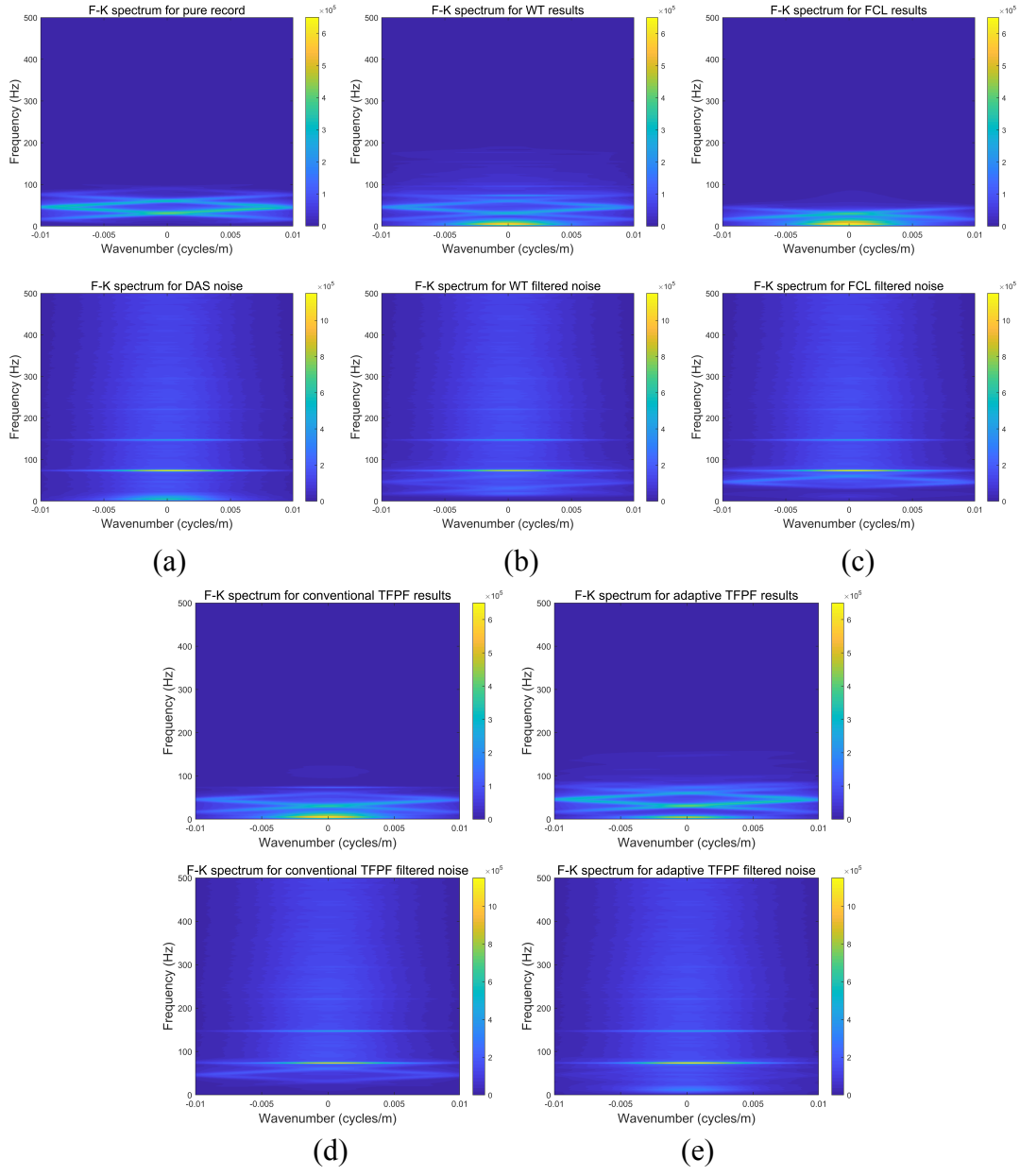

Fig. 11. F-K domain analysis for the processing results. (a) F-K spectrum of synthetic record and field background noise. (b)-(e) F-K spectrum of denoising results for WT, FCL, conventional TFPF and adaptive TFPF, respectively.

For further investigating the efficiency, the denoising results are analyzed in the frequency domain, and the F-K spectra for the corresponding results are shown in Fig. 11. Notably, the recovered signals obtained by the competing algorithms all have conspicuous amplitude losses or property changes, especially for the results of FCL. In contrast, as shown in Fig. 11(e), the results for adaptive TFPF have the most similar characteristics with the clean record in the f-k spectrum. Therefore, the results are consistent with the findings discussed above that the proposed adaptive TFPF can recover the effective events without obvious amplitude loss. All these results indicate that the adaptive TFPF has better performance than the competing algorithms.

On this basis, we also investigate the denoising capability for different algorithms under different conditions, and the improved SNR and RMSE, shown in eqs. (11) and (12), are calculated for detailed comparisons.

$$SNR(dB) = 10\log_{10}\left(\frac{\sum_{i=1}^{N}\sum_{j=1}^{M}u_0(i,j)^2}{\sum_{i=1}^{N}\sum_{j=1}^{M}(u(i,j)-u_0(i,j))^2}\right), \tag{11}$$

$$RMSE = \sqrt{\frac{1}{MN}\sum_{i=1}^{N}\sum_{j=1}^{M}(u(i,j)-u_0(i,j))^2}. \tag{12}$$

where u and u_0 represent the clean records and denoising results, whereas M and N are the dimensions of the analyzed data. Moreover, the corresponding quantitative comparison results for *SNR* and *RMSE* are shown in Table 2. It is demonstrated that the adaptive TFPF has the largest improved *SNR* and the smallest *RMSE*, whereas an improvement of over 11 dB could be obtained even for -10 dB records. Thus, by combining the aforementioned results, we can suggest that adaptive TFPF, over a 6 dB increment than the competing algorithm, is efficient in eliminating the DAS background while considering signal preservation.

Table 2. Averaged SNR and RMSE comparisons for different denoising results.

Original record (dB)	WT		FCL		TFPF		Adaptive TFPF	
	SNR (dB)	RMSE	SNR (dB)	RMSE	SNR (dB)	RMSE	SNR (dB)	RMSE
-10	-3.41	0.209	-6.55	0.300	-4.22	0.230	1.48	0.119
-5	2.17	0.110	0.86	0.128	1.73	0.116	5.81	0.072
0	6.12	0.070	3.23	0.097	7.05	0.063	12.43	0.034
5	8.98	0.050	7.14	0.062	9.93	0.045	13.57	0.030

Field DAS record processing results

To analyze the efficiency of the proposed algorithm, we also applied it to a field DAS record. The field DAS data, shown in Fig. 12(a), were severely affected by the interference, and some of the reflection events were buried in the strong background noise. For comparison, WT, conventional TFPF, and adaptive TFPF were applied to the field DAS record, and the processing results are shown in Figs. 12(b) to (d), respectively. Apparently, the processing results for WT and conventional TFPF falls short of expectations, and noise reduction performance and continuity for the recovered signals still need to be further improved. In Fig. 12(d), the adaptive TFPF method can suppress the background noise more effectively, and the recovered events have better continuity and smoothness by comparing with competing methods. On this basis, the removed noise records for different algorithms are also analyzed in detail. The results are shown in Fig. 13. Notably, obvious residual signal components exist in the results for WT and conventional TFPF [shown in Figs. 13(a) and (b)]. On the contrary, there is almost no signal-leakage energy in Fig. 13(c), which demonstrates that the adaptive TFPF has few adverse effects on the recovered events during the denoising procedure. As discussed above, we found that adaptive TFPF has better performance in noise attenuation with consideration of signal preservation, even under low SNR conditions.

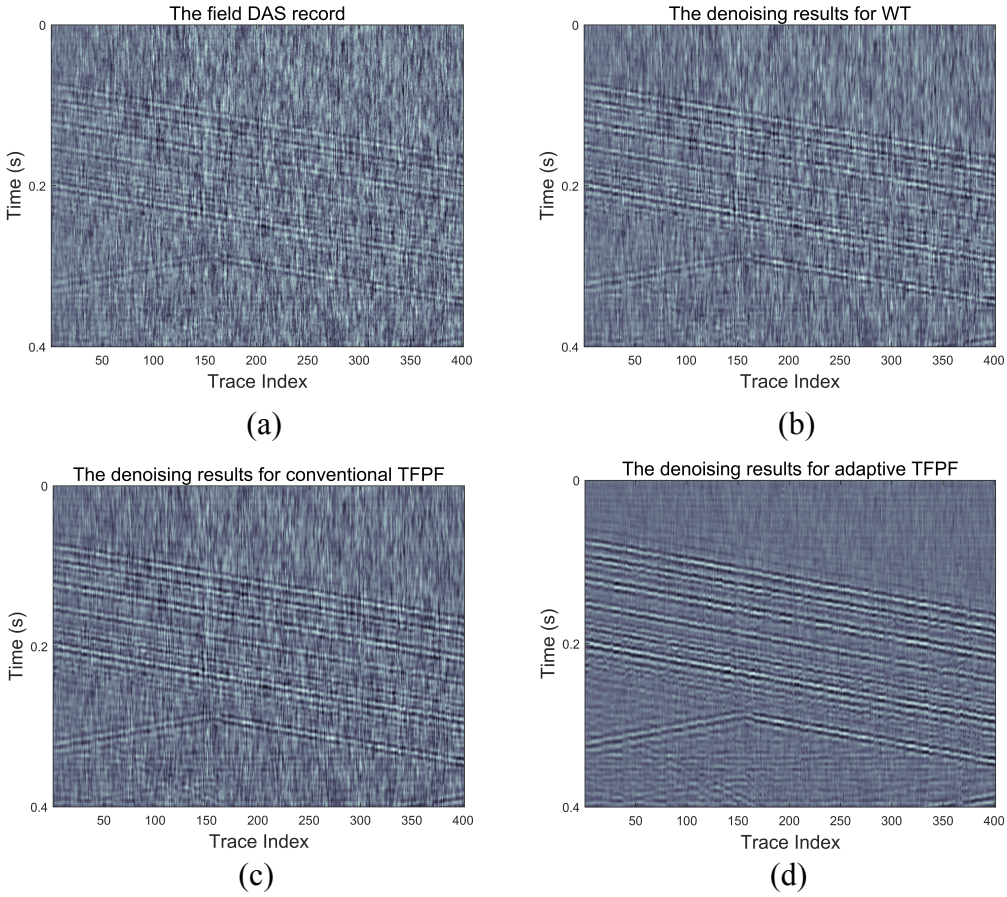

Fig. 12. Denoising results of field DAS data. (a) The field DAS record. (b) Denoising results of WT. (c) Denoising results of conventional TFPF. (d) Denoising results of adaptive TFPF.

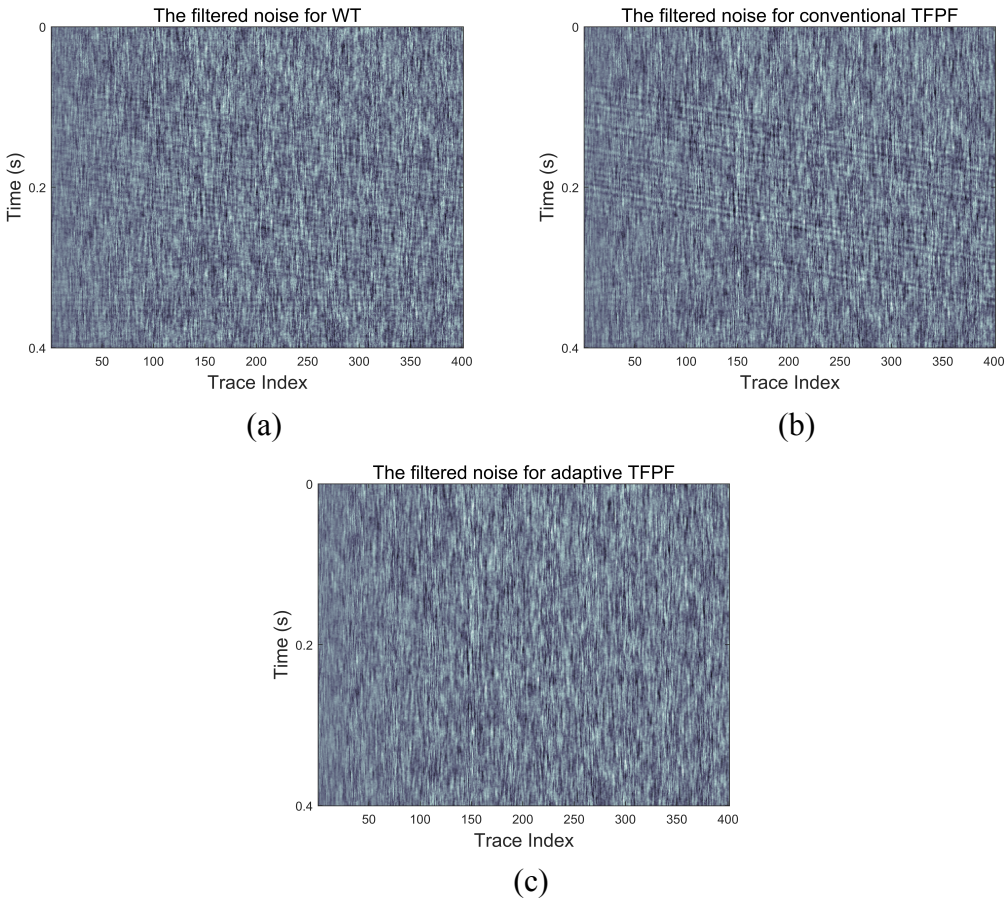

Fig. 13. The comparisons of filtered noise. (a) Filtered noise for WT. (b) Filtered noise for conventional TFPF. (c) Filtered noise for adaptive TFPF.

CONCLUSION

In this study, we analyzed the properties of the DAS background noise, mainly concentrated in stationarity and PSD. The dataset used is collected under the course of exploration industry. By analyzing DAS records, the results indicate that the background noise is local-stationary. It means that the stationarity for the noise series in the short period is high, and the non-stationary portions are all below 20%. Moreover, the experimental results indicate that DAS noise is broadband in nature, which is different from the traditional understanding in seismic data processing. Additionally, the stationarity and PSD properties for the reflection signals were also investigated. The corresponding results indicate that the reflection signal, whose energy was mainly concentrated in the range of 0–70 Hz, display a more significant non-stationary component. Based on these findings, we propose an improved TFPF filtering method that utilizes the stationarity and PSD analysis results to adaptively determine the filtering parameters. Specifically, we can separate the processing data as signal and noise segments by investigating the stationary features. Subsequently, filtering

parameters are adaptively determined for each segment to get better performance in noise reduction and signal restoration. Different competing algorithms were applied to verify the efficiency of the proposed method, both on synthetic and field DAS records. It is shown that the adaptive TFPF algorithm outperforms the other competing methods, with an increment of over 10 dB in synthetic data processing. Furthermore, it is noticed that the recovered reflection events also have better properties in terms of continuity and smoothness after applying adaptive TFPF algorithm. In summary, we can get the point that the proposed adaptive TFPF method can effectively attenuate DAS background noise and improve the quality of the analyzed data, especially in complicated noise conditions. From this viewpoint, we can infer that the adaptive TFPF algorithm may have further application in the field of DAS data denoising and processing.

ACKNOWLEDGMENTS

This work was financially supported by the National Natural Science Foundation of China under Grants 41974143 and the Foundation for Youth Excellence of the Jilin Science and Technology Bureau under Grants 20200104116. All authors declare that there is no potential sources of conflict of interest. Tie Zhong and Xintong Dong contributed equally to this work.

REFERENCES

Ardekani, I.T. and Abdulla, W.H., 2013. Stochastic modelling and analysis of filtered-xleast-mean-square adaptation algorithm. IET Sign. Process., 7: 486-496.

Azerad, P., Bouharguane, A. and Crouzet, J.F., 2012. Simultaneous denoising and enhancement of signals by a fractal conservation law. Commun. Nonlinear. Sci., 17: 867-811.

Bayram, M. and Baraniuk, R., 2000. Multiple window time-varying spectrum estimation. In: Fitzgerald, W.J. (Ed.), Nonlinear and Nonstationary Signal Processing. Cambridge University Press, Cambridge: 292-316.

Bellefleur, G , Schetselaar, E., Wade, D., White, D., Enkin, R. and Schmitt, D.R., 2020. Vertical seismic profiling using Distributed Acoustic Sensing (DAS) with scatter-enhanced fibre-optic cable at the Cu-Au new Afton Porphyry deposit, British Columbia, Canada. Geophys. Prosp., 68: 313-333.

Binder, G., Titov A., Liu Y., Simmons, J. and Monk, D., 2020. Modeling the seismic response of individual hydraulic fracturing stages observed in a time-lapse DAS VSP survey. Geophysics, 85(4): T225-T235.

Boashash, B. and Mesbah, M., 2004. Signal enhancement by time-frequency peak filtering. IEEE Transact. Signal Process., 52: 929-937.

Chatfield, C., 2003. The Analysis of Time Series: An Instruction, 6th ed.. Chapman and Hall/CRC Press, Houston.

Correa, J., Egorov, A., Tertyshnikov, K., Bona, A. and Pevzner, R., 2017. Analysis of signal to noise and directivity characteristics of DAS VSP at near and far offsets - a CO2CRC Otway Project data example. The Leading Edge, 36: 994a1–994a7.

Daley, T.M., Miller, D.E., Dodds, K., Cook, P. and Freifeld, B. M., 2016. Field testing of modular borehole monitoring with simultaneous distributed acoustic sensing and geophone vertical seismic profiles at Citronelle, Alabama. Geophys. Prosp., 64: 1318-1334.

Dong, X., Li, Y., Wu, N., Tian, Y. and Yu, P., 2018. The S-STK/LTK algorithm for arrival time picking of microseismic signals. J. Geophys. Engineer., 15: 1484-1491.150

Egorov, A., Correa, J., Bona, A., Pevzner, R., Tertyshnikov, K., Glubokovskikh, S., Puzyev, V. and Gurevich, B., 2018. Elastic full waveform inversion of vertical seismic profile data acquired with distributed acoustic sensors. Geophysics, 83(3), R273-R281.

Flandrin, P., Rilling, G., Goncalves, P., 2014. Empirical mode decomposition as a filter bank. IEEE Signal Process. Lett., 11: 112-114.

Gang, Y., Zhidong, C., Yuanzhong, C., Wang, X., Zhang, Q., Li, Y., Wang, Y., Liu, C., Zhao, B. and Joe, G., 2018. Borehole seismic survey using multimode optical fibers in a hybrid wireline. Measurement, 125: 694-703.

Gotz, J., Luth, S., Henninges, J. and Thomas, R., 2018. Vertical seismic profiling using daisy-chained deployment of fibre-optic cables in four wells simultaneously - case study at the Ketzin carbon dioxide storage site. Geophys. Prosp., 66: 1201-1214.

Harris, K., White, D. and Samson, C., 2017. Imaging the Aquistore reservoir after 36 kilotonnes of CO2 injection using distributed acoustic sensing. Geophysics, 82(6): M81-M96.

Hartog, A.H., 2018. An Introduction to Distributed Optical Fibre Sensing. CRC Press, Houston. Jiang C., Li Y., Wu N., et al. 2011. Radial-trace time–frequency peak filtering based on correlation integral. IEEE Geosci. Remote Sens. Lett., 11: 1594-1598.

Karrenbach, M., Cole, S., Ridge, A., Boone, K., Kahn, D., Rich, J., Silver, K. and Langto, D., 2019. Fiber-optic distributed acoustic sensing of microseismicity, strain and temperature during hydraulic fracturing. Geophysics, 84(1): D11-D23.

Kobayashi, Y., Uematsu, Y., Mochiji, S. and Xue, Z., 2020. A field experiment of walkaway distributed acoustic sensing vertical seismic profile in a deep and deviated onshore well in Japan using a fibre optic cable deployed inside coiled tubing. Geophys. Prosp., 68: 501-520.

Li, G., Li, Y. and Yang, B., 2017. Seismic exploration random noise on land: modeling and application to noise suppression. IEEE Transact. Geosci. Remote Sens., 55: 4668-4681.

Mateeva, A., Lopez, J., Potters, H., Mestayer, J., Cox, B., Kiyashchenko, D., Wills, P., Grandi, S., Hornman, K., Kuvshinov, B., Berlang, W., Yang, Z. and Detomo, R., 2014. Distributed acoustic sensing for reservoir monitoring with vertical seismic profiling, Geophys. Prosp., 62: 679-692.

Martins, H.F., Fernández-Ruiz, M., Costa, L., Williams, E. and Gonzalez-Herraez. M.,, 2019. Monitoring of remote seismic events in metropolitan area fibers using distributed acoustic sensing (DAS) and spatiotemporal signal processing. Optical Fiber Communication Conference, San Diego.

Meng, F., Li, Y., Wu, N. and Lin, H., 2015. A fractal conservation law for simultaneous denoising and enhancement of seismic data. IEEE Geosci. Remote Sens. Lett., 12: 374-378.

Moghtaderi, A., Flandrin, P. and Borgnat, P., 2013. Trend filtering via empirical mode decompositions. Computat. Statist. Data Analys., 58: 114-126.

Parker, T., Shatalin, S. and Farhadiroushan, M. 2014. Distributed acoustic sensing - a new tool for seismic applications. First Break , 32: 61-69.

Poletto, F., Finfer, D., Corubolo, P. and Farina, B., 2016. Dual wavefields from distributed acoustic sensing measurements. Geophysics, 81(6): D585-D597.

Riedel, M., Cosma, C., Enescu, N., Koivisto, E., Komminaho, K and Vaittinen, K., 2018. Underground vertical seismic profiling with conventional and fiber-optic systems for exploration in the Kylylahti Polymetallic Mine, Eastern Finland. Minerals, 8(11): 538.

Rodrigue, I.V. and Wuestefeld, A., 2020. Strain microseismics: Radiation patterns, synthetics, and moment tensor resolvability with distributed acoustic sensing in isotropic media. Geophysics, 85(3): KS101-KS114.

Soto, M.A., Ramírez, J. and Thévenaz, A.L., 2016. Intensifying the response of distributed optical fibre sensors using 2D and 3D image restoration. Nature Commun., 7: 10870.

Souza, D., Chanussot, J., Favre, A.C. and Borgnat, P., 2013. A new nonparametric method for testing stationarity based on trend analysis in the time marginal distribution. IEEE International Conference on Acoustics, Speech and Signal Processing, 320-324.151

Spikes, K.T., Tisato, N., Hess, T.E. and Holt, J.W., 2019. Comparison of geophone and surface-deployed distributed acoustic sensing seismic data. Geophysics, 84(2): A25-A29.

Thomson, D.J., 1982. Spectrum estimation and harmonic analysis. Proceedings of the IEEE, 70: 1055-1096.

Verdon, J.P., Horne, S.A., Clarke, A., Stock, A.L. and Kendall, J.M., 2020. Microseismic monitoring using a fiber-optic distributed acoustic sensor array. Geophysics, 85(3): KS89-KS99.

Wu, N., Li, Y. and Yang, B.J., 2011. Noise attenuation for 2-D seismic data by radial-trace time-frequency peak filtering. IEEE Geosci. Remote Sens. Lett., 8: 874-878.

Zhang, C., Li, Y., Lin, H. and Yang, B., 2015. Signal preserving and seismic random noise attenuation by Hurst exponent based time–frequency peak filtering. Geophys. J. Internat., 203: 901-909.

Zhong, T., Li, Y., Wu, N., Nie, P. and Yang, B., 2015. Statistical analysis of background noise in seismic prospecting. Geophys. Prosp., 60: 1161-1174.

Zhong, T., Li, Y., Wu, N., Nie, P. and Yang, B., 2015. A study on the stationarity and Gaussianity of the background noise in land seismic prospecting. Geophysics, 80(4): V67-V82.

Zhong, T., Zhang, S., Li, Y. and Yang, B., 2019. Simulation of seismic-prospecting random noise in the desert by a Brownian-motion-based parametric modeling algorithm. Compt. Rend. Geosci., 351: 10-16.